Transplanet: A web service dedicated to modeling of planetary ionospheres

P.-L. Blelly, A. Marchaudon, M. Indurain, O. Witasse, J. Amaya, B. Chide, N. Andre, V. Genot, A. Goutenoir, M. Bouchemit

Planetary and Space Science 169 (2019) 35–44

Contents lists available at ScienceDirect

Planetary and Space Science

journal homepage: www.elsevier.com/locate/pss

Transplanet: A web service dedicated to modeling of planetary ionospheres

P.-L. Blelly [a,*], A. Marchaudon [a], M. Indurain [a], O. Witasse [b], J. Amaya [c], B. Chide [d,a], N. André [a], V. Génot [a], A. Goutenoir [a], M. Bouchemit [a]

[a] Institut de Recherche en Astrophysique et Planétologie (IRAP), Université de Toulouse, CNRS, CNES, UPS, Toulouse, France
[b] European Space Agency, ESTEC - Scientific Support Office, Keplerlaan 1, Noordwijk, 2200, AG, the Netherlands
[c] Centre for Mathematical Plasma Astrophysics (CmPA), KU Leuven, Celestijnenlaan 200b - Box 2400, 3001, Leuven, Belgium
[d] Institut Supérieur de l'Aéronautique et de l'Espace, Toulouse, France

ARTICLE INFO

Keywords:
Planetary ionospheres
IPIM modeling
Web service
Virtual observatory

ABSTRACT

We present a new web service (http://transplanet.irap.omp.eu/) dedicated to the modeling of planetary ionospheres. Thanks to the development made for IRAP ionospheric model IPIM, it uses a unified description of the different ionized environments (presently Venus, Earth, Mars and Jupiter). The service provides a complete set of parameters characterizing these environments, including the concentration, velocities, temperatures, production rates of the different ions and electron heating rates. It is based on a modular approach allowing for selection of species, date of simulation and location. It is intended to be a support tool to data processing and analysis and we describe how simulation results can be used for such a purpose. The output format has been chosen to ease the interface with external data processing or vizualization tools, including online services. This web service is an open service which aims at providing users with the most relevant and consistent description of the couplings in planetary space environments and it will evolve in a way to increase user control on the simulation through a simplified Human-machine interface (HMI).

1. Introduction

The Planetary SpaceWeather Services (PSWS) (http://planetaryspaceweather-europlanet.irap.omp.eu/) of the Europlanet 2020-RI project (André et al., 2018) aim at providing information about the solar wind properties, following solar perturbations throughout the Solar System, as well as giving the most consistent description of the different space environments of planets and how each of them is affected by the solar wind. In such a context, the Transplanet service (http://transplanet.irap.omp.eu/) developed in the frame of PSWS is a web interface allowing online runs of the physics-based IRAP Plasmasphere Ionosphere Model (IPIM) (Marchaudon and Blelly, 2015; Blelly et al., 2005) in its planetary-independent version. Transplanet aims at providing consistent and detailed description of the ionized atmosphere, called ionosphere, of a selection of planets in the Solar System. A user of Transplanet can thus choose to model the ionosphere of Venus, Earth, Mars or Jupiter. The ionosphere is one of the key interaction region between the planetary environment and solar radiation and solar wind. It is critical for Planetary Weather activities in terms, for example, of radio signal propagation through atmosphere and radio-occultation experiment.

Important assets of the Transplanet service are:

- to give access to a large set of parameters (density, temperature, velocity, heat flux) self-consistently solved for all the main ionospheric species taking into account realistic inputs, such as the solar flux
- to allow comparative studies at different planets
- to provide modeling results easily downloadable from the Transplanet website in Common Data Format (CDF)
- to allow direct visualization of the results in the Automated Multi-Dataset Analysis (AMDA) webtool (Jacquey et al., 2010) developed by Centre de données de la Physique des Plasmas (CDPP) through IVOA SAMP protocol
- to compare simulation results with observations from different spacecraft and even from some ground-based facilities in the terrestrial case (e.g. Incoherent Scatter Radar), whose data are also available in AMDA

At the best of our knowledge, the Transplanet service has currently no equivalent elsewhere. Although a large set of ionosphere models (physical and empirical) are also accessible for online run at the Community

* Corresponding author.
E-mail address: pierre-louis.blelly@irap.omp.eu (P.-L. Blelly).

https://doi.org/10.1016/j.pss.2019.02.008
Received 7 November 2018; Received in revised form 14 January 2019; Accepted 21 February 2019
Available online 15 March 2019

Coordinated Modeling Center (CCMC) website (https://ccmc.gsfc.nasa.gov), they are only available for the terrestrial case.

Section 2 will briefly introduce the main features of the IPIM model and will describe some of the strategic developments made for the planetary-independent version. Section 3 will then describe the Transplanet interface publicly available at (http://transplanet.irap.omp.eu/): request and results webpages and its connection to the AMDA webtool (http://amda.cdpp.eu/). Some applications will then be presented and discussed in Section 4, followed by a description of the future improvements planned for the service in Section 5.

2. Description of the model

2.1. General characteristics

IPIM is a legacy of the high latitude ionosphere model (TRANSCAR) and Mars ionosphere model (TRANSMARS) family models (Diloy et al., 1996; Blelly et al., 2005; Morel et al., 2004; Leblanc et al., 2006) with substantial improvements, which are thoroughly described in (Marchaudon and Blelly, 2015), the first being that the transport equations for the ionized species are based on a 16 moment approximation (Blelly and Schunk, 1993). Fig. 1 presents the synopsis of IPIM ionosphere model and in this paper, we will focus on the main features with regard to the application we foresee through Transplanet. The model used in Transplanet project is an updated version of the Earth model described in (Marchaudon and Blelly, 2015): it is built in a modular way, leading to a core model that is independent from the planet. This core model corresponds to the part delimited by the red line in Fig. 1 and it is based on two

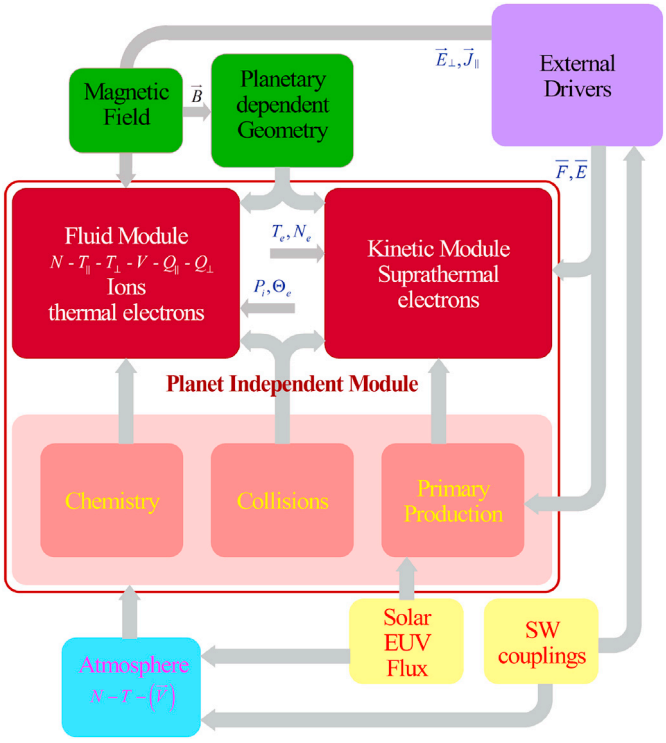

Fig. 1. Synopsis of IPIM model. The core of the model (red boxes) is built with a planet independent architecture and is based on a two-side coupling between fluid and kinetic models: thermal electron temperature and density are provided to the kinetic model and ion production rate and thermal electron heating rate are provided to the fluid model. The planet dependent characteristics are provided externally like the magnetic geometry and orbitography (green boxes), the neutral atmosphere: concentration (N), temperature (T) and optionally velocity ($\vec{V}$) (blue box) or the drivers (violet box). The solar activity is accounted for through the EUV flux (yellow box). (For interpretation of the references to color in this figure legend, the reader is referred to the Web version of this article.)

modules which separate the plasma between thermal and suprathermal contributions.

Both modules solve one dimensional (1D) transport equations and thus require a spatial grid which is determined by the characteristics of the planet; this dependency is represented by the two green boxes in Fig. 1. Basically, depending on whether a magnetic field is present or not, the spatial grid is adapted as followed:

- without magnetic field, the grid used is vertical (spherical coordinates),
- in case of intrinsic magnetic field, the grid used is field aligned (interhemispheric grid in case of closed field lines).

The thermal plasma is composed of the different ions considered in the simulation and the thermal electrons, and is treated through the fluid module. For every ion considered, this module solves the time-dependent 1D transport equations of the density, the velocity, the temperature (parallel and perpendicular if a magnetic field is present) and the heat flux (components for the parallel and perpendicular temperatures if applicable). This fluid module accounts for the chemistry and the collisions between the ions and the neutrals.

The suprathermal electron are obtained from the kinetic module which solves the steady state transport equation of the distribution function of this population, according to a multistream approach (Oran and Strickland, 1978). This module accounts for the collisions on the neutrals and excitation and ionization of these species either by solar radiation illumination or electron impact.

Fluid and kinetic modules are coupled so that the kinetic module provides the total production rates of the ions resulting from the primary production stemed from the photoionization and the secondary production stemed from the suprathermal electron impact on the neutrals, as well as the thermal electron heating due the interaction with the suprathermal electrons.

All the interaction processes (collisions, chemical reactions) are described in sub-modules (salmon-colored boxes) which only contain planet independent algorithms. They are adjusted in the initialization phase of the model according to the neutral species considered in the simulation. This is provided by the atmosphere module (blue box in Fig. 1), which is specific to every considered planet, but with a common interface developed to allow the modular approach in IPIM. The neutral atmosphere is characterized by the concentration profiles of the different species considered in the simulation, the temperature profile and, if possible, the neutral wind. It is provided either through an "empirical model" based on data post-processing using analytical formulation or a "generic profile model". In latter case, the atmosphere "model" is an analytical integration of barometric law with respect to a reference altitude for which neutral atmosphere measurements are available; it uses a formulation similar to the one in the theoretical thermosphere model (Rees and Fuller-Rowell, 1988) of the COSPAR International Reference Atmosphere (CIRA) model (Rees and COSPAR International Reference Atmosphere, 1986), with a neutral temperature fitted according to a Bates' profile (Bates, 1959).

With the given neutral species and the solved ions, the initialization phase of the model determines which collision processes and chemical reactions should be retained and chooses the collision frequencies and ionization cross sections which are necessary for the model to run.

The other planet dependent feature is the orbitography, which is provided through NAIF system and Spice kernels (Acton, 1996; Acton et al., 2018) for all the planets we consider in Transplanet. Based on this orbitography, the code determines the geometry with respect to the Sun (green box) and together with the solar conditions provided externally, i.e. the solar flux and solar wind couplings with the planetary environment (yellow boxes in Fig. 1), we can compute the primary production of the ions.

The external drivers (violet box in Fig. 1) resulting from these couplings are specific to each planet. In the case of the Earth, due to the

magnetosphere, the magnetic activity and the precipitation and electrodynamics patterns will characterize these coupling inputs. In the case of Mars or Venus, the direct inputs of electrons from the solar wind will characterize these couplings.

2.2. Solar flux

One of the main inputs to the model is the EUV solar flux responsible for atmosphere's photoionization. The IPIM model can account for any solar flux model, in general based on measurements at 1 Astronomical Unit (AU) (Earth's orbit) and re-scaled to the position of the considered planet. In the primary version of the web service, the EUV Flux Model for Aeronomic Calculations (EUVAC) (Richards et al., 1994) is the only one available. This model provides a solar flux on 22 wavelength intervals (continuum) and 17 lines between 1.9 nm and 103 nm. It is based on a solar EUV minimum reference spectrum and the dependency on the solar activity is obtained through weighted linear function of $F_{10.7}$.

2.3. Planet dependent inputs

2.3.1. Venus

Atmosphere. The neutral atmosphere model presently used for density and temperature is the Venus Atmosphere model VTS-3 (Hedin et al., 1983). This model is derived from Pioneer Venus Mission and is built with the same analytical functions used for Earth Mass Spectrometer Incoherent Scatter radar (MSIS) atmosphere model (Hedin et al., 1977). It does not give any information on the dynamics (no winds) but it describes the thermal structure of the main neutral species: CO_2, O, CO, He and N.

Magnetic field. No magnetic field is presently considered.

2.3.2. Earth

Atmosphere. The neutral atmosphere model used is the Naval Research Laboratory Mass Spectrometer Incoherent Scatter radar (NRLMSISE-00) (Picone et al., 2002) for density (neutral species considered: N_2, O_2, O, N and H) and temperature and the Horizontal Wind Model (2007 version) (HWM07) (Drob et al., 2008; Emmert et al., 2008) for winds (horizontal zonal and meridional components).

Magnetic field. The magnetic field is derived from the International Geomagnetic Reference Field (IGRF) (Thébault et al., 2015). Using the eight first coefficients of the IGRF model, we compute the characteristics of the equivalent eccentric tilted dipole, which is used to define the magnetic field line geometry.

2.3.3. Mars

Atmosphere. The Neutral atmosphere is taken from the Mars Climate Database (MCD) (Forget et al., 1999; Millour et al., 2015), which provides density (neutral species considered: CO_2, O_2, N_2, O, H and CO), temperature and velocities (horizontal zonal and meridional components) for different solar conditions.

Magnetic field. No magnetic field is presently considered. The former model version TRANSMARS had a mode to solve for the induced magnetic field resulting from the interaction between the solar wind and the Mars upper atmosphere (Shinagawa and Cravens, 1989). However, this mode put strong constrains on the geometry which made it difficult to account for in the initial version of the unified model. As a result, we preferred not to include such an option, though we are working on it for a future version.

2.3.4. Jupiter

Atmosphere. The atmosphere is given by the "generic profile model" described previously with characteristics adjusted from the data obtained during the descent of the Galileo Probe (Table 5 from (Seiff et al., 1998)). It provides the concentration of the main neutral species: H_2, H, He and CH_4 species with their temperature, but there is no information on the dynamics (no winds).

Magnetic field. The magnetic field is given by the VIPAL model (Hess et al., 2011) from which, similarly to the Earth, we use the eight first coefficients to derive the equivalent eccentric tilted dipole.

3. Description of the web interface

3.1. "Request Run" tab

The user interface has been conceived to be easy to use and intuitive and can be found on the tab entitled "Request Run". For description, we divide the interface into three parts.

3.1.1. Planet selection

First, the user has to choose the planet by clicking on the corresponding icon (panel (a) in Fig. 2). As a simulation run can last a few hours, the user will then have to fill in an email address where a message, containing a link to the data, will be sent when the run results will be available. An optional and succinct description of the run is also possible and recommended. Depending on the selected planet, the set of neutral and ion species is automatically updated to match the planet's atmosphere. Currently, only the ion species can be modified (tick boxes) and depending on those modified, the IPIM model will adapt the chemical scheme to only solve equations for the chosen ions.

3.1.2. Conditions of the simulation

Second, the user has to define the simulation by providing the start date and time (Universal Time (UT)), the duration of the simulation run and the time step (in second) between two consecutive output results (panel (b) in Fig. 2). Then the user chooses successively the different models used as inputs to IPIM for kinetic processes, magnetic field if any (Earth and Jupiter) and atmosphere. Currently, only energy degradation from photoionization is available for all planets.

3.1.3. Selection of the location

The condition of the simulation being defined, the user may wish to make simulations at different locations with the same condition. For that (panel (c) in Fig. 2), he can choose up to 10 different positions. The possible coordinate system allowed is only planetographic (lon, lat) for Venus and Mars, while for Earth and Jupiter, three other systems, based on the magnetic field, are also available: magnetic (lon, lat), invariant (Magnetic Local Time (MLT), L) and local magnetic (MLT, lat).

3.2. "View Results" tab

All the requested runs are archived and publicly available on the results web page, listing all the past requested runs (http://transplanet.irap.omp.eu/index.html, see Fig. 3), with the more recent ones at the top of the page. When the results are ready, the user will receive an email with a dedicated link, which is also available through this results web page. Each run is briefly described in one line and the user can click on two different icons at the right-hand side of the line: one for downloading the run results through the form of a zipped file containing as many files as simulated positions (all in CDF format), and one to send the result of the first simulated position via Simple Application Messaging Protocol (SAMP) (Taylor et al., 2015) to the AMDA (Génot et al., 2014) web tool for rapid visualization. Before this operation, the user needs to be first connected to a hub. A user guide for plotting Transplanet results is provided as supplementary material. An example of electron density and temperature AMDA plots for a run at Venus, which will be described thoroughly in section 4, is presented in Fig. 4.

4. An application to venus environment

IPIM is now used on a routine basis and simulations for Earth (Marchaudon et al., 2018) and Mars (Sánchez-Cano et al., 2018) environments have already been published. So, in this section, we

Fig. 2. Snapshot of the "Request Run" interface (http://transplanet.irap.omp.eu/create.html): section (a) corresponds to the selection of the planet, section (b) to the conditions of the run (date and duration) and section (c) to the location of the run.

concentrate on a simulation corresponding to the latest development for Venus and we present some key parameters which can be obtained through the simulations. We choose to compare a simulation using Transplanet interface to measurements obtained with Venus Express Radio Science (VeRa) (Häusler et al., 2006) onboard Venus Express Mission (VEX) (Svedhem et al., 2007). The atmosphere and ionosphere of Venus were sounded by VeRa at 2.3 and 8.4 GHz (the S and X bands, respectively) during the first occultation season from mid-July to the end of August 2006 and some profiles were presented in (Pätzold et al., 2007). In this section, we want to show how the results from Transplanet simulation can be used to analyze the dataset.

4.1. IPIM simulations

We choose DOY196 profile obtained on July 15, 2006 at local time 15:20 and latitude −4.7° with a solar zenith angle (SZA) of 50° (Fig. 4 from (Pätzold et al., 2007)). Due to the slow rotation, the ionosphere is more likely dependent on the solar zenithal angle than the local time, so we run two 24-h-duration simulations with Transplanet: one at longitude −50° and latitude −4.7° corresponding to the morning sector and the other at longitude +50° and latitude −4.7° corresponding to the afternoon sector. From these simulations, we extracted the profiles corresponding to SZA 50° and compared them to the measurements (Fig. 5):

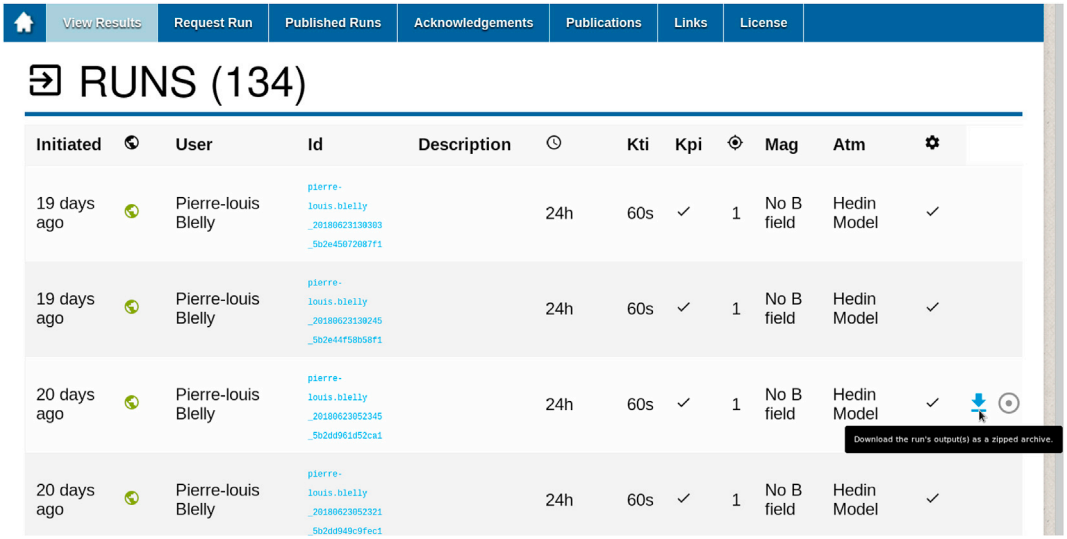

Fig. 3. Snapshot of the "View Results" interface (http://transplanet.irap.omp.eu/index.html).

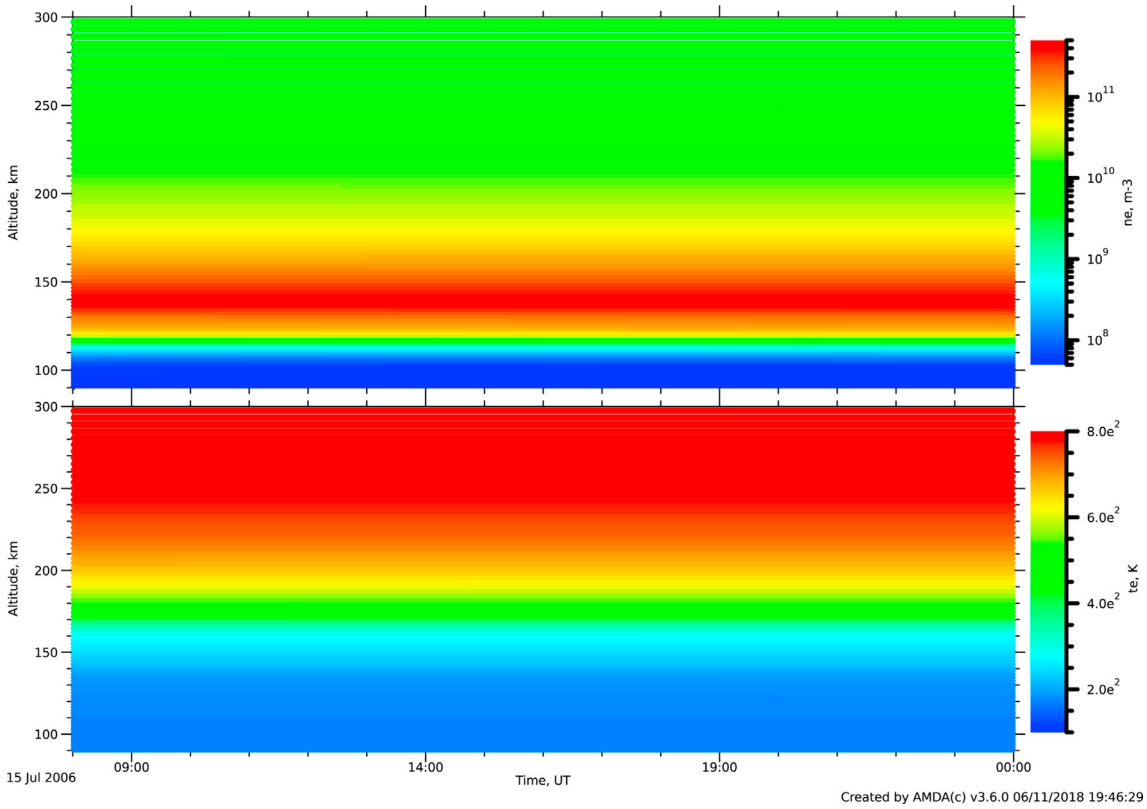

Fig. 4. Color panels representing the temporal evolution of the electron concentration (top panel in logarithmic scale) and the electron temperature (bottom panel in linear scale), between 90 and 300 km for a simulation at Venus on July 15, 2006. (For interpretation of the references to color in this figure legend, the reader is referred to the Web version of this article.)

the first simulation gives a profile for local time 8:40 and the second simulation a profile for local time 15:20. As expected, the slow rotation of the planet inhibits the dependency on local time and both simulations are quite similar. As shown on Fig. 5 (in logarithmic scale) or Fig. 8 (in linear scale), both simulation differs by less than 5% in the region of interest, so we will focus on simulation for longitude +50° which corresponds to the same local time as the observation.

On the left panel of Fig. 5, we have plotted data from VeRa (with dots) with the two modeled electron density profiles. We have also plotted the different ionized species profiles corresponding to simulation with longitude +50°. On the right panel, we have plotted the temperatures derived from the simulation (O^+ ion in red and e^- in green) and neutral temperature from VTS-3 model (in blue) for longitude +50°. Data and simulation compare very well: in VeRa data, the maximum of concentration is reached around 143 km (V_2 peak as referenced by (Pätzold et al., 2007)) with a value of about 3.8×10^{11} m^{-3}, while in the simulation the maximum is reached around 139 km with the same value of 3.8×10^{11} m^{-3}. There is a slight difference of about 4 km in the location of the V_2 peak that we discuss later. Unsurprisingly, O_2^+ ion is found to be the major species in the lower part of the ionosphere (below 180 km)

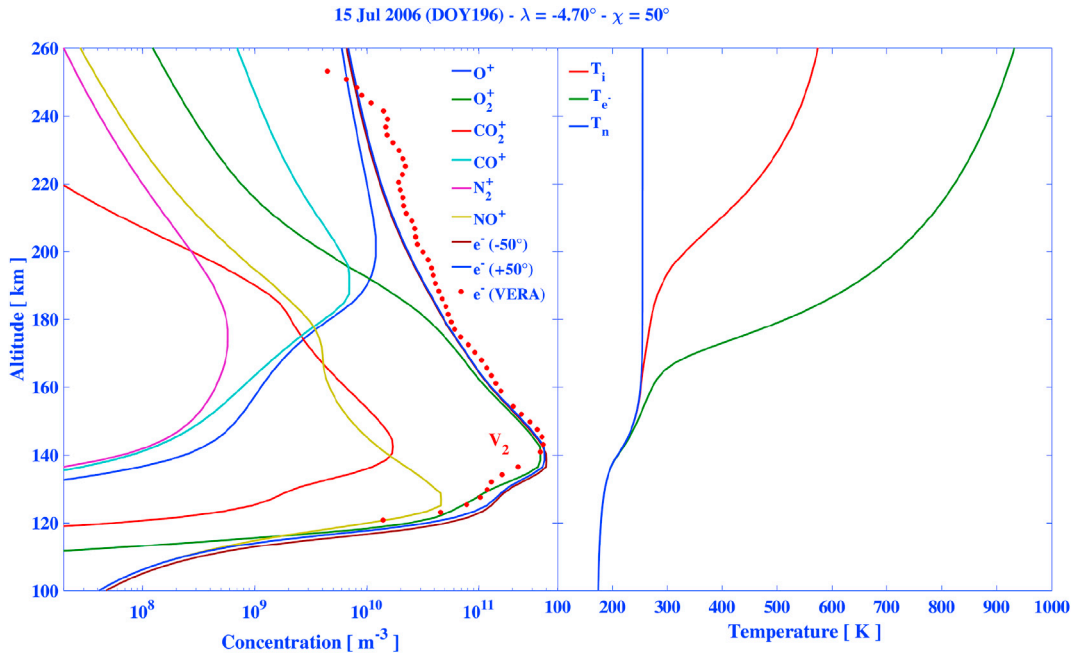

Fig. 5. Profiles of ionized species concentration (left) and temperature (right) in Venus ionosphere obtained through Transplanet for 15 Jul 2006 (DOY196) compared to the electron concentration data for this day from VeRa experiment onboard Venus Express.

with a concentration comparable to the one of NO^+ below the V_2 peak. O^+ ion becomes the major ion above approximately 190 km with a concentration of about 10^{11} m^{-3} at the altitude of transition from molecular to atomic ions. From measurements, (Pätzold et al., 2007), locates the ionopause around 260 km, meaning that there is no influence of an induced magnetic field below this altitude and thus chemistry and diffusion should be the dominant processes below 200 km.

Fig. 6 gives some insights on the chemical processes. On left panel, we have plotted the production rates for the different species obtained from the simulation which only accounts for photoionization, based on the EUVAC solar flux model. We have computed the loss of electrons by chemistry (electron dissociative recombination reactions) which are plotted with green dots. We clearly see that the photochemical equilibrium prevails up to about 180 km and mainly corresponds to a primary production of CO_2^+ ion. The predominance of O_2^+ ion results from chemistry and the V_2 layer may be characterized by a Chapman layer as a first approximation. On the right panel, we have plotted the different neutral species profiles given by the VTS-3 model. The atmosphere is made of more than 90% of CO_2 up to 130 km and the fact that N_2 is about 4% around 120 km explains why NO^+ ion concentration is significant.

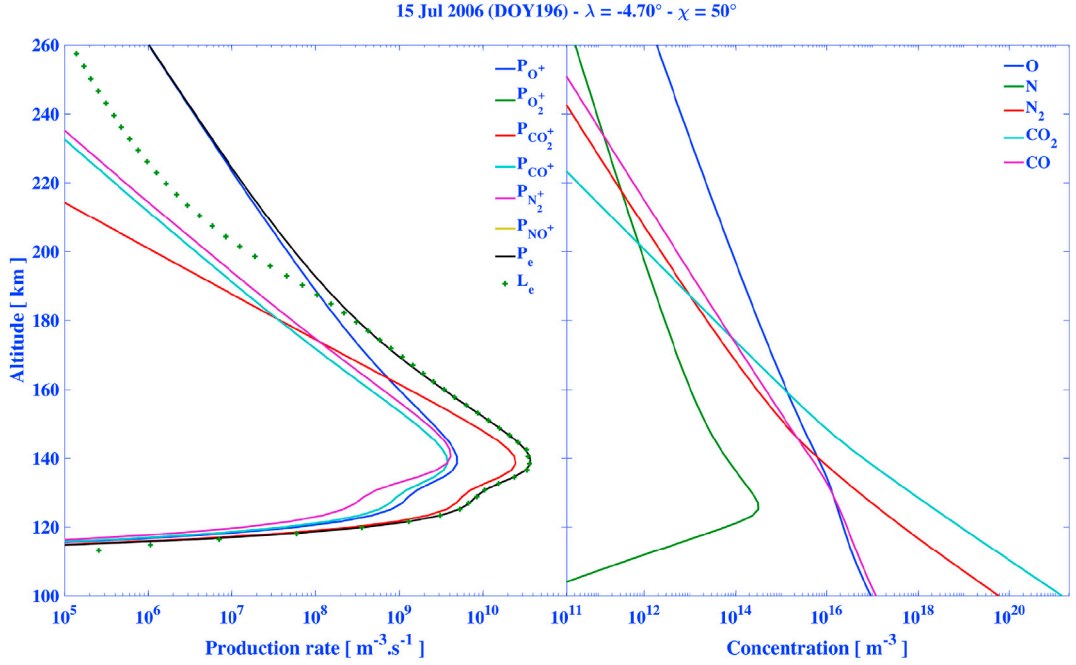

Fig. 6. Profiles of ion production rates, electron production and loss rates from the simulation (left) and neutral density concentration from VTS-3 (right) in Venus atmosphere.

4.2. Analysis and correction

In this section, we present how the difference of about 4 km in the location of the maximum of concentration between the data and the simulation can be corrected by modifying some critical parameters like the atmosphere concentration.

In a Chapman layer, the altitude of the maximum of production is colocated with the altitude of the maximum of concentration. Fig. 7 presents, on left panel, the electron concentration of Fig. 5 around the peak in linear scale. The simulation for longitude −50° has the lowest maximum. Simulation for longitude +50° is about 1 km above the former and VERA is around 4 km above the latter. We have also plotted on the left panel, the electron concentration for longitude +50° shifted by 3.7 km. We see that there is a very good match with the data, indicating that the maximum of production has to be translated upward.

Chapman layer is associated with the Chapman production model (see e.g. (Blelly et al., 2007)), which brings out the main features of photoionization:

- flux is absorbed according to a Beer-Lambert law and is a function of the neutral column density along the line of sight to the Sun (Chapman function);
- production rate is proportional to local concentration and flux at a given altitude.

The total production is obtained by integration over the wavelengths of the solar spectrum. However, this model does not account for secondary production which comes from photoelectrons (electrons emerging from photoionization) with energies above ionization thresholds. Considering that these secondary electrons are mainly produced in the region where their mean free path is small, that is to say in dense regions, we can parametrize these secondary electrons by the column density and thus write for every species n an ad hoc representation of the production $P_n(z)$ which accounts for the main features presented above:

$$P_n(z) = \beta_n N_n(z) \Lambda_n(\rho(z)) \tag{1}$$

where β_n is a photoionization frequency of neutral species n and represents the mean ionization efficiency of the solar flux for this species, N_n is the concentration of this species and $\Lambda_n(\rho)$ is a function which characterizes the efficiency of the production along the path of solar radiations and as such can be identified as a deposition function. This path is parametrized by ρ which is the column density of the atmosphere along the line of sight to the Sun. When ρ is low, Λ_n is close to 1 as there is almost no absorption of the flux and when ρ is high, Λ_n decreases rapidly to 0, similarly to what occurs with the Chapman function in the Chapman production model. Λ_n may reach a maximum above 1 if secondary electrons are efficient to produce the species n.

From this expression, we can derive the electron production rate:

$$P_e(z) = \sum_n P_n(z) = \sum_n \beta_n N_n(z) \Lambda_n(\rho(z)) \tag{2}$$

For a given geometry (SZA) and given environmental conditions (atmosphere and solar activity), we can derive this function from the individual production rates given by the simulation. We can then consider that these functions are unchanged if the conditions are unchanged. Namely, if we consider that the neutral temperature is unchanged and that the neutral concentration of the different species is changed by a factor x, Λ_n are correct as long as we change ρ consistently. From Eq. (2), we see that the only way to shift upward the production is to change the concentration of the different neutral species so that the maximum of production is shifted.

On the right panel of Fig. 7, we have plotted the local atmosphere scale height (mainly CO_2) together with the different locations of the maximum of electron concentration. At these altitudes, 3.7 km represents about 80 % of the scale height, which means that such a shift correspond to a reduction of the atmosphere by a factor of about 2. The consequence is that there is no possibility to shift upward the maximum of production if the atmosphere is kept unchanged. On the other hand, if we change all the species by a factor x, then the production P_e becomes:

$$P_e(z) = x \sum_n \beta_n N_n(z) \Lambda_n(x\rho(z)) \tag{3}$$

So, we see that x is a free parameter which can be optimized to adjust the location of the maximum of the production P_e. In practice, we can consider only CO_2 and N_2 in the process as they are the main species

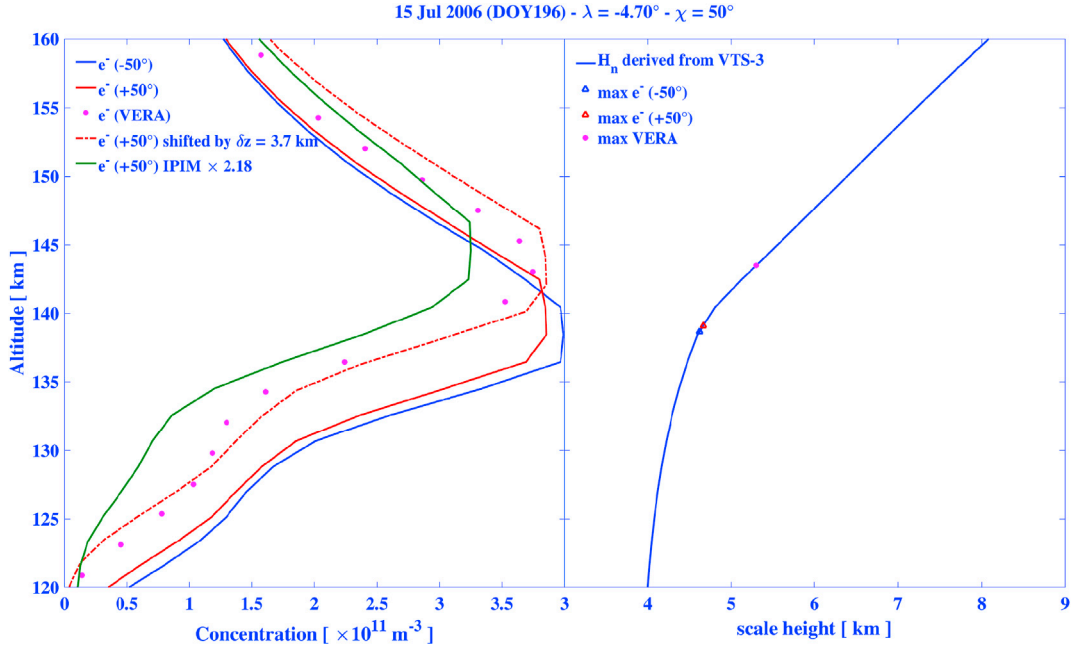

Fig. 7. Left panel: profiles of electron concentration around the maximum in linear scale for VeRa data (magenta dots), IPIM simulations (blue, red and green) and translated IPIM simulation (dashed red); right panel: profile of local neutral scale height with location of the different maximum of electron concentration. (For interpretation of the references to color in this figure legend, the reader is referred to the Web version of this article.)

contribution to the production. From Eq. (1) and production rate profiles (Fig. 6) we can derive, for longitude +50° simulation, $\beta_{CO_2} = 5.45 \times 10^{-7}$ s^{-1} and $\beta_{N_2} = 2.21 \times 10^{-6}$ s^{-1} and the function Λ_n for these two species which are plotted on left panel of Fig. 8 (CO_2 in red and N_2 in blue). The vertical green lines represent the limits in ρ within which we will optimize the factor x and the vertical dashed green line represents the location of the initial maximum of production for longitude +50° simulation. On right panel, we have plotted in red the altitude of the maximum of production using expression 3 for a given factor x; the reference simulation corresponds to $x = 1$. From this curve, we see that shifting upward by 3.7 km the maximum of production requires to multiply the atmosphere by a factor $x = 2.18$. As a comparison, the blue line represents the factor which would be needed to keep unchanged the concentration at the maximum by just using the barometric law (associated to scale height H_n).

We have made a simulation with IPIM using a factor $x = 2.18$ on the atmosphere and the green curve on left panel of Fig. 7 is the result we get. We clearly see that the maximum is located at the right position, meaning that the neutral atmosphere at the time of observation is higher by a factor about 2 than the model predicts. However, VeRa maximum is about 15% higher than the simulation, which means that the solar flux used in the simulation is lower than the true one by about 30%. To check that point, we run IPIM model with Flare Irradiance Spectral Model (FISM) as solar flux model for that day and the correction factor $x = 2.18$ for the atmosphere. The maximum concentration is obtained at the same altitude and its value is within 5% from the value from VeRa; therefore, EUVAC is actually responsible for the difference between the simulation and the observations. A new optimization step should be necessary for a fine tuning of the parameters, but this is out of the scope of this study.

Through this use case, we show first the ability of IPIM to accurately model planetary environments and then how Transplanet service can be used for comparison with basic ionospheric observations. The outputs from the simulations provide insight on the detailed description of the ionospheric structure and thermodynamics, and they can help to optimize atmosphere and solar flux parameters, which are generally estimated through empirical models.

5. Future developments of the Transplanet service and concluding remarks

The Transplanet service is only useful if it provides a user friendly interface which offers a scientific added value. As we were in a feasibility phase, the initial HMI was built in relation to some few parameters, which we allowed the control from the potential users. However, we now want to go further and for the future, we intend to make new developments to the model and to the Transplanet web interface.

In the short run, we will concentrate on the easiest and quickest developments and on adding new features to the interface. First, the flexible approach used to select the ions in the IPIM chemical scheme, will also be unleashed for neutrals (they are grayed out in the present interface, see Fig. 3).

Concerning the production, though we can use any model, we presently limit to the EUVAC model. So, we will also add new solar flux models:

- the Hinteregger model (Hinteregger, 1981) which uses different reference spectra as the EUVAC model but with the same wavelength resolution. The dependency on $F_{10.7}$ is basically the same, but the weighted functions differs.
- the Flare Irradiance Spectral Model (FISM) (Richards et al., 1994). This model is based on Thermosphere Ionosphere Mesosphere Energetics and Dynamics mission (TIMED) and Upper Atmosphere Research Satellite (UARS) measurements and is provided between 0.1 nm and 190 nm with a resolution of 1 nm. The solar flux is available on a daily basis since 1947.

Beside this, the use case presented in the previous section, has put forward the necessity for allowing a correction factor on atmosphere and solar flux as input to simulations. We will add the possibility to upload correction factors in the simulation.

Moreover, the current version only allows for energy degradation from photoionization, though the kinetic module can account for electron precipitation (currently grayed tick box). We will quickly give the possibility to the user to use magnetospheric inputs for the terrestrial

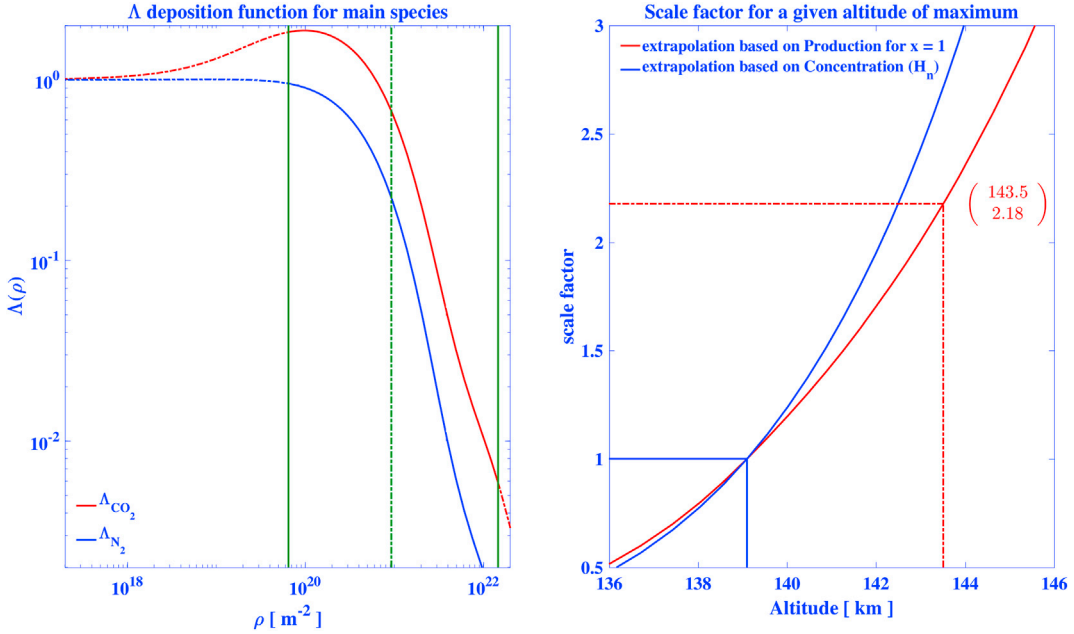

Fig. 8. Left panel:deposition function Λ for CO_2 and N_2 species for longitude +50° simulation. The vertical green lines represent the limits in ρ within which factor x is optimized and the vertical dashed green line represents the location of the initial maximum of production. right panel: atmosphere scale factor x as a function of the altitude of the maximum of production derived from optimization of Eq. (3) and the solution is shown by the red dashed lines. As a comparison, the blue line represents the factor which would be needed to keep unchanged the concentration at the maximum by just using the barometric law (associated to scale height H_n). (For interpretation of the references to color in this figure legend, the reader is referred to the Web version of this article.)

version of the model by adding precipitation model from (Hardy et al., 1987). We will also extent the capacity of the model by adding the possibility to upload a user defined precipitation flux in the simulation.

Electrodynamics couplings are important in the Earth case, so we will unbridle plasma transport due to convection by allowing for convection models obtained from SuperDARN convection observations (e.g. (Cousins and Shepherd, 2010) or (Thomas and Shepherd, 2018)).

We will also add new coordinate systems to give access to a position at the planet's surface either from its local time or from its solar zenithal angle (SZA). This type of information can be clearly useful for planets without magnetic field and to compare to radio-occultation experiment as the one presented in the previous section.

We will increase the available number of magnetic field and atmosphere models for the different planets, for instance the new Jovian magnetic field model based on Juno's first nine orbits (Connerney et al., 2018). These developments are planned on a more long-term basis, as validation of each of these models will be needed through a few runs of IPIM. Finally in the longer run, we will add an induced magnetic field module to Mars and Venus. We will also do our best to offer a Saturn-version of the model. This may prove more difficult as we will need to take into accounts the rings in the plasma dynamics of the planet. Efforts will also be made to promote the service like making all runs available through EPN-TAP (Erard et al., 2014), in particular via the Virtual European Solar and Planetary Access (VESPA) portal (http://vespa.obspm.fr).

In conclusion, the results presented in the previous section as well as the IPIM papers already published confirm the capability of the IPIM model to adequately reproduce the main processes affecting the different solar system planets. We still foresee numerous developments for the model itself and for the associated web interface and we hope that it will encourage potential users to apply the model in support of their own observations, especially in the case of planetary missions.

Acknowledgement

The original IPIM Model was developed by P.-L. Blelly and A. Marchaudon at IRAP (CNRS and Toulouse University) and is a property of Centre National de la Recherche Scientifique (CNRS). Simulation results of the Transplanet models have been provided by the Planetary Space Weather Services through their public Online Runs system (http://transplanet.irap.omp.eu/). Transplanet is a service developed by CNRS/IRAP/CDPP for the Planetary Space Weather Services of the Europlanet 2020 Research Infrastructure. Europlanet 2020 RI has received funding from the European Union's Horizon 2020 research and innovation programme under grant agreement No 654208. This work is also supported by the Programme National Soleil Terre (PNST) from Institut des Sciences de l'Univers of CNRS (INSU/CNRS) co-funded by Centre National d'Études Spatiales (CNES).

Appendix A. Supplementary data

Supplementary data to this article can be found online at https://doi.org/10.1016/j.pss.2019.02.008.

Acronyms

1D	one dimensional
AMDA	Automated Multi-Dataset Analysis
AU	Astronomical Unit
CCMC	Community Coordinated Modeling Center
CDF	Common Data Format
CDPP	Centre de données de la Physique des Plasmas
CIRA	COSPAR International Reference Atmosphere
EUV	Extreme UltraViolet flux
EUVAC	EUV Flux Model for Aeronomic Calculations
FISM	Flare Irradiance Spectral Model
HWM07	Horizontal Wind Model (2007 version)
IGRF	International Geomagnetic Reference Field
HMI	Human-machine interface
IPIM	IRAP Plasmasphere Ionosphere Model
MCD	Mars Climate Database
MSIS	Mass Spectrometer Incoherent Scatter radar
NRLMSISE-00	Naval Research Laboratory Mass Spectrometer Incoherent Scatter radar
PSWS	Planetary Space Weather Services
SAMP	Simple Application Messaging Protocol
SZA	solar zenith angle
TIMED	Thermosphere Ionosphere Mesosphere Energetics and Dynamics mission
TRANSCAR	high latitude ionosphere model
TRANSMARS	Mars ionosphere model
UARS	Upper Atmosphere Research Satellite
MLT	Magnetic Local Time
UT	Universal Time
VeRa	Venus Express Radio Science
VEX	Venus Express Mission
VESPA	Virtual European Solar and Planetary Access

References

Acton, C.H., 1996. Ancillary data services of NASA's navigation and ancillary information facility. Planet. Space Sci. 44, 65–70. https://doi.org/10.1016/0032-0633(95)00107-7.

Acton, C., Bachman, N., Semenov, B., Wright, E., 2018. A look towards the future in the handling of space science mission geometry. Planet. Space Sci 150, 9–12. https://doi.org/10.1016/j.pss.2017.02.013.

André, N., Grande, M., Achilleos, N., Barthélémy, M., Bouchemit, M., Benson, K., Blelly, P.-L., Budnik, E., Caussarieu, S., Cecconi, B., Cook, T., Génot, V., Guio, P., Goutenoir, A., Grison, B., Hueso, R., Indurain, M., Jones, G.H., Lilensten, J., Marchaudon, A., Matthiä, D., Opitz, A., Rouillard, A., Stanislawska, I., Soucek, J., Tao, C., Tomasik, L., Vaubaillon, J., 2018. Virtual planetary space weather services offered by the Europlanet H2020 research infrastructure. Planet. Space Sci. 150, 50–59. https://doi.org/10.1016/j.pss.2017.04.020.

Bates, D.R., 1959. Some problems concerning the terrestrial atmosphere above about the 100 km level. Proceedings of the Royal Society of London Series A 253, 451–462. https://doi.org/10.1098/rspa.1959.0207.

Blelly, P.-L., Schunk, R.W., 1993. A comparative study of the time-dependent standard 8-, 13- and 16-moment transport formulations of the polar wind. Ann. Geophys. 11, 443–469.

Blelly, P.-L., Lathuillère, C., Emery, B., Lilensten, J., Fontanari, J., Alcaydé, D., 2005. An extended TRANSCAR model including ionospheric convection: simulation of EISCAT observations using inputs from AMIE. Ann. Geophys. 23, 419–431. https://doi.org/10.5194/angeo-23-419-2005.

Blelly, P.-L., Alcaydé, D., Ionosphere, 2007. In: Kamide, Yohsuke, Chian, Abraham C.-L. (Eds.), Handbook Of the Solar-Terrestrial Environment. Springer, Berlin, pp. 189–220. https://doi.org/10.1007/11367758_8.

Connerney, J.E.P., Kotsiaros, S., Oliversen, R.J., Espley, J.R., Joergensen, J.L., Joergensen, P.S., Merayo, J.M.G., Herceg, M., Bloxham, J., Moore, K.M., Bolton, S.J., Levin, S.M., 2018. A new model of jupiter's magnetic field from Juno's first nine orbits. Geophys. Res. Lett. 45, 2590–2596. https://doi.org/10.1002/2018GL077312.

Cousins, E.D.P., Shepherd, S.G., 2010. A dynamical model of high-latitude convection derived from SuperDARN plasma drift measurements. J. Geophys. Res. 115 (A14), A12329. https://doi.org/10.1029/2010JA016017.

Diloy, P.-Y., Robineau, A., Lilensten, J., Blelly, P.-L., Fontanari, J., 1996. A numerical model of the ionosphere, including the E-region above EISCAT. Ann. Geophys. 14, 191–200. https://doi.org/10.1007/s00585-996-0191-7.

Drob, D.P., Emmert, J.T., Crowley, G., Picone, J.M., Shepherd, G.G., Skinner, W., Hays, P., Niciejewski, R.J., Larsen, M., She, C.Y., Meriwether, J.W., Hernandez, G., Jarvis, M.J., Sipler, D.P., Tepley, C.A., O'Brien, M.S., Bowman, J.R., Wu, Q., Murayama, Y., Kawamura, S., Reid, I.M., Vincent, R.A., 2008. An empirical model of the Earth's horizontal wind fields: HWM07. J. Geophys. Res. 113 (A12), A12304. https://doi.org/10.1029/2008JA013668.

Emmert, J.T., Drob, D.P., Shepherd, G.G., Hernandez, G., Jarvis, M.J., Meriwether, J.W., Niciejewski, R.J., Sipler, D.P., Tepley, C.A., 2008. DWM07 global empirical model of upper thermospheric storm-induced disturbance winds. J. Geophys. Res. 113 (A12), A11319. https://doi.org/10.1029/2008JA013541.

Erard, S., Cecconi, B., Le Sidaner, P., Berthier, J., Henry, F., Molinaro, M., Giardino, M., Bourrel, N., André, N., Gangloff, M., Jacquey, C., Topf, F., 2014. The EPN-TAP protocol for the planetary science virtual observatory. Astronomy and Computing 7, 52–61. https://doi.org/10.1016/j.ascom.2014.07.008. 1407.5738.

Forget, F., Hourdin, F., Fournier, R., Hourdin, C., Talagrand, O., Collins, M., Lewis, S.R., Read, P.L., Huot, J.-P., 1999. Improved general circulation models of the Martian atmosphere from the surface to above 80 km. J. Geophys. Res. 104, 24155–24176. https://doi.org/10.1029/1999JE001025.

Génot, V., André, N., Cecconi, B., Bouchemit, M., Budnik, E., Bourrel, N., Gangloff, M., Dufourg, N., Hess, S., Modolo, R., Renard, B., Lormant, N., Beigbeder, L., Popescu, D., Toniutti, J.-P., 2014. Joining the yellow hub: uses of the Simple application messaging protocol in space physics analysis tools. Astronomy and Computing 7, 62–70. https://doi.org/10.1016/j.ascom.2014.07.007.

Hardy, D.A., Gussenhoven, M.S., Raistrick, R., McNeil, W.J., 1987. Statistical and functional representations of the pattern of auroral energy flux, number flux, and conductivity. J. Geophys. Res. 92, 12275–12294. https://doi.org/10.1029/JA092iA11p12275.

Häusler, B., Pätzold, M., Tyler, G.L., Simpson, R.A., Bird, M.K., Dehant, V., Barriot, J.-P., Eidel, W., Mattei, R., Remus, S., Selle, J., Tellmann, S., Imamura, T., 2006. Radio science investigations by VeRa onboard the Venus express spacecraft, planet. Space Sci 54, 1315–1335. https://doi.org/10.1016/j.pss.2006.04.032.

Hedin, A.E., Reber, C.A., Newton, G.P., Spencer, N.W., Salah, J.E., Evans, J.V., Kayser, D.C., Alcaydé, D., Bauer, P., Cogger, L., 1977. A global thermospheric model based on mass spectrometer and incoherent scatter data MSIS. I - N2 density and temperature. J. Geophys. Res. 82, 2139–2147. https://doi.org/10.1029/JA082i016p02139.

Hedin, A.E., Niemann, H.B., Kasprzak, W.T., Seiff, A., 1983. Global empirical model of the Venus thermosphere. J. Geophys. Res. 88, 73–83. https://doi.org/10.1029/JA088iA01p00073.

Hess, S.L.G., Bonfond, B., Zarka, P., Grodent, D., 2011. Model of the Jovian magnetic field topology constrained by the Io auroral emissions. J. Geophys. Res. 116, A05217. https://doi.org/10.1029/2010JA016262.

Hinteregger, H.E., 1981. Representations of solar EUV fluxes for aeronomical applications. Adv. Space Res. 1, 39–52. https://doi.org/10.1016/0273-1177(81)90416-6.

Jacquey, C., Génot, V., Budnik, E., Hitier, R., Bouchemit, M., Gangloff, M., Fedorov, A., Cecconi, B., André, N., Lavraud, B., Harvey, C., Dériot, F., Heulet, D., Pallier, E., Penou, E., Pinçon, J.L., AMDA, 2010. Automated multi-dataset analysis: a web-based service provided by the CDPP. Astrophysics and Space Science Proceedings 11, 239–247. https://doi.org/10.1007/978-90-481-3499-1_16.

Leblanc, F., Witasse, O., Winningham, J., Brain, D., Lilensten, J., Blelly, P.-L., Frahm, R.A., Halekas, J.S., Bertaux, J.L., 2006. Origins of the martian aurora observed by spectroscopy for investigation of characteristics of the atmosphere of Mars (SPICAM) on board Mars express. J. Geophys. Res. 111, A09313. https://doi.org/10.1029/2006JA011763.

Marchaudon, A., Blelly, P.-L., 2015. A new interhemispheric 16-moment model of the plasmasphere-ionosphere system: IPIM. J. Geophys. Res. 120, 5728–5745. https://doi.org/10.1002/2015JA021193.

Marchaudon, A., Blelly, P.-L., Grandin, M., Aikio, A., Kozlovsky, A., I, V., 2018. IPIM modeling of the ionospheric F2 layer depletion at high latitudes during a high-speed stream event. J. Geophys. Res. 123 https://doi.org/10.1029/2018JA025744.

Millour, E., Forget, F., Spiga, A., Navarro, T., Madeleine, J.-B., Montabone, L., Pottier, A., Lefevre, F., Montmessin, F., Chaufray, J.-Y., Lopez-Valverde, M.A., Gonzalez-Galindo, F., Lewis, S.R., Read, P.L., Huot, J.-P., Desjean, M.-C., 2015. MCD/GCM development team, the Mars climate Database (MCD version 5.2). European Planetary Science Congress 10, EPSC2015–E2438.

Morel, L., Witasse, O., Warnant, R., Cerisier, J.-C., Blelly, P.-L., Lilensten, J., 2004. Diagnostic of the dayside ionosphere of Mars using the Total Electron Content measurement by the NEIGE/Netlander experiment: an assessment study, Planet. Space Sci 52, 603–611.

Oran, E.S., Strickland, D.J., 1978. Photoelectron flux in the earth's ionosphere, Planet. Space Sci 26, 1161–1177. https://doi.org/10.1016/0032-0633(78)90056-9.

Pätzold, M., Häusler, B., Bird, M.K., Tellmann, S., Mattei, R., Asmar, S.W., Dehant, V., Eidel, W., Imamura, T., Simpson, R.A., Tyler, G.L., 2007. The structure of Venus' middle atmosphere and ionosphere. Nature 450, 657–660. https://doi.org/10.1038/nature06239.

Picone, J.M., Hedin, A.E., Drob, D.P., Aikin, A.C., 2002. NRLMSISE-00 empirical model of the atmosphere: statistical comparisons and scientific issues. J. Geophys. Res. 107, 1468. https://doi.org/10.1029/2002JA009430.

Rees, D., Fuller-Rowell, T.J., 1988. The CIRA theoretical thermosphere model. Adv. Space Res. 8, 27–106. https://doi.org/10.1016/0273-1177(88)90039-7.

Rees, D., COSPAR International Reference Atmosphere, 1986. Part 1: thermosphere models. Adv. Space Res. 8.

Richards, P.G., Fennelly, J.A., Torr, D.G., 1994. EUVAC: a solar EUV flux model for aeronomic calculations. J. Geophys. Res. 99, 8981–8992. https://doi.org/10.1029/94JA00518.

Sánchez-Cano, B., Lester, M., Witasse, O., Blelly, P.-L., Indurain, M., Cartacci, M., González-Galindo, F., Vicente-Retortillo, A., Cicchetti, A., Noschese, R., 2018. Spatial, seasonal, and solar cycle variations of the martian total electron content (TEC): is the TEC a good tracer for atmospheric cycles? J. Geophys. Res. 123 https://doi.org/10.1029/2018JE005626.

Seiff, A., Kirk, D.B., Knight, T.C.D., Young, R.E., Mihalov, J.D., Young, L.A., Milos, F.S., Schubert, G., Blanchard, R.C., Atkinson, D., 1998. Thermal structure of Jupiter's atmosphere near the edge of a 5-μm hot spot in the north equatorial belt. J. Geophys. Res. 103, 22857–22890. https://doi.org/10.1029/98JE01766.

Shinagawa, H., Cravens, T.E., 1989. A one-dimensional multispecies magnetohydrodynamic model of the dayside ionosphere of Mars. J. Geophys. Res. 94, 6506–6516. https://doi.org/10.1029/JA094iA06p06506.

Svedhem, H., Titov, D.V., McCoy, D., Lebreton, J.-P., Barabash, S., Bertaux, J.-L., Drossart, P., Formisano, V., Häusler, B., Korablev, O., Markiewicz, W.J., Nevejans, D., Pätzold, M., Piccioni, G., Zhang, T.L., Taylor, F.W., Lellouch, E., Koschny, D., Witasse, O., Eggel, H., Warhaut, M., Accomazzo, A., Rodriguez-Canabal, J., Fabrega, J., Schirmann, T., Clochet, A., Coradini, M., 2007. Venus express the first european mission to Venus, planet. Space Sci 55, 1636–1652. https://doi.org/10.1016/j.pss.2007.01.013.

Taylor, M.B., Boch, T., Taylor, J., 2015. SAMP, the Simple application messaging protocol: letting applications talk to each other. Astronomy and Computing 11, 81–90. https://doi.org/10.1016/j.ascom.2014.12.007. 1501.01139.

Thébault, E., Finlay, C.C., Alken, P., Beggan, C.D., Canet, E., Chulliat, A., Langlais, B., Lesur, V., Lowes, F.J., Manoj, C., Rother, M., Schachtschneider, R., 2015. Evaluation of candidate geomagnetic field models for IGRF-12. Earth Planets Space 67, 112. https://doi.org/10.1186/s40623-015-0273-4.

Thomas, E.G., Shepherd, S.G., 2018. Statistical patterns of ionospheric convection derived from mid-latitude, high-latitude, and polar SuperDARN HF radar observations. J. Geophys. Res. 123, 3196–3216. https://doi.org/10.1002/2018JA025280.